Available online at www.sciencedirect.com
ScienceDirect
Journal of Crystal Growth 296 (2006) 150–158
JOURNAL OF CRYSTAL GROWTH
www.elsevier.com/locate/jcrysgro

Modeling ammonothermal growth of GaN single crystals: The role of transport

S. Pendurti[a,*], Q.-S. Chen[b], V. Prasad[a]

[a]Department of Mechanical Engineering, Florida International University, EAS 2710, 10555, W. Flagler Street, Miami, FL 33174, USA
[b]Institute of Mechanics, Chinese Academy of Sciences, 15 Bei Si Huan Xi Road, Beijing 100080, China

Received 28 May 2006; received in revised form 24 July 2006; accepted 28 July 2006
Communicated by R. Fornari
Available online 10 October 2006

Abstract

Single crystal gallium nitride (GaN) is an important technological material used primarily for the manufacture of blue light lasers. An important area of contemporary research is developing a viable growth technique. The ammonothermal technique is an important candidate among many others with promise of commercially viable growth rates and material quality. The GaN growth rates are a complicated function of dissolution kinetics, transport by thermal convection and crystallization kinetics. A complete modeling effort for the growth would involve modeling each of these phenomena and also the coupling between these. As a first step, the crystallization and dissolution kinetics were idealized and the growth rates as determined purely by transport were investigated. The growth rates thus obtained were termed 'transport determined growth rates' and in principle are the maximum growth rates that can be obtained for a given configuration of the system. Using this concept, a parametric study was conducted primarily on the geometric and the thermal boundary conditions of the system to optimize the 'transport determined growth rate' and determine conditions when transport might be a bottleneck.

PACS: 07.05.Tp

Keywords: A1. Convection; A1. Fluid flows; A1. Growth models; A2. Ammonothermal growth; B1. GaN

1. Introduction

The use of gallium nitride (GaN) in the manufacture of blue/green light LEDs, lasers and high power electronic devices has given rise to the demand for commercially viable processes for growth of single crystal GaN material. Presently, GaN epitaxial layers are grown on sapphire or SiC substrates, but a large lattice mismatch makes the production of bulk GaN substrates imperative. The growth of bulk GaN material is technologically difficult owing to the high melting point of GaN and the dissociation of GaN into Ga and N_2, well before the melting point. Consequently, traditional techniques involving growth from the melt and sublimation involve very high temperatures and pressures that are not realizable with the equipment available presently. A variety of techniques are being tried out to produce bulk substrates. High nitrogen pressure liquid phase growth (HNPLPG) [1], where nitrogen is used to saturate liquid gallium at a high temperature and pressure of 1500 °C and 10–15 Kbar, respectively. Instead of pure nitrogen, ammonia or a mixture of nitrogen and ammonia have been used to lower the operating temperature and pressure. A closely related sodium flux method has been developed to further lower the temperature and pressure [2]. A promising method is the ammonothermal technique pioneered by Dwilinski et al. [3,4] and further being developed by Ketchum and Kolis [5], Purdy [6], and Yoshikawa et al. [7]. The ammonothermal technique is drawn from the hydrothermal technique widely used to grow quartz. In this technique, supercritical water was kept in a tightly sealed

*Corresponding author. Tel.: +13053486827; fax: +13053481401.
E-mail address: pendurti@fiu.edu (S. Pendurti).

0022-0248/$ - see front matter © 2006 Elsevier B.V. All rights reserved.
doi:10.1016/j.jcrysgro.2006.07.034

Nomenclature

c_p	specific heat capacity
C	GaN intermediate concentration in solution
C_2	inertial resistance coefficient in the porous media
C_μ	turbulence viscosity coefficient
d_p	average diameter of particle in nutrient layer
D	dynamic diffusion coefficient of solute
$\vec{g}$	gravity vector
G_b	turbulent kinetic energy production due to buoyancy
G_k	turbulence kinetic energy production due to velocity gradients
k_s	thermal conductivity in solid
k_f	thermal conductivity in fluid
k_{eff}	effective thermal conductivity in fluid and porous zones
k_{por}	conductivity in porous zone
k	turbulent kinetic energy
K	permeability of the porous bed
M	molecular weight of intermediate species (kg/kmol)
$\vec{n}$	normal vector
p	pressure
Pr	Prandtl number
Pr_t	turbulence Prandtl number
q_w	heat flux at wall
T	temperature
T_0	reference temperature
T_w	wall temperature
t	time
U	velocity parallel to wall
V	Specific volume
u_i	component of velocity in direction 'i'
$\vec{v}$	velocity vector
x_i	ith Cartesian coordinate
y	normal distance from wall

Greek letters

α_ε	inverse Prandtl number for turbulent dissipation
α_k	inverse Prandtl number for turbulent kinetic energy
β_f	thermal expansion coefficient of fluid
ε	turbulent energy dissipation
ε_{bed}	porosity of the nutrient layer
μ	viscosity
ρ	density
$\bar{\bar{\tau}}$	viscous part of stress tensor

Subscripts

c	quantity corresponding to critical point
eff	effective quantity
f	fluid
p	quantities at point 'P' near wall
turb	turbulent related quantity
lam	laminar related quantity

Superscripts

*	non-dimensional quantity

vessel at a pressure of 2–4 Kbar and temperature 500 °C. A porous baffle divides the vessel into a lower chamber and an upper growth chamber. The lower chamber contains a porous bed of quartz powder, and the upper growth chamber contains quartz seeds. The supercritical water in the lower chamber dissolves quartz from the porous bed, and is driven into the upper chamber by thermal convection currents. Since the upper chamber is at a lower temperature, the water there is supersaturated with quartz, hence quartz is deposited on the seeds resulting in single crystal growth. The ammonothermal growth of GaN is an extension of this basic idea with the solvent being ammonia instead of water. One of the major issues in ammonothermal growth is the growth rate. So far crystals of size 1 mm have been grown after 5 days of growth through the process of spontaneous nucleation [8]. Seeded growth has been reported with a net weight gain of the order of grams after 4 days of growth, though this information is unpublished. While crystal quality is of paramount importance, an important area of research is to enhance the growth rate at least to the levels of hydrothermal growth of quartz (1–2 mm/day), so that large-scale growth of GaN substrates is viable. The growth rate in the ammonothermal process is determined by the rate of three phenomena that take place in series—dissolution of the GaN powder in the supercritical ammonia, transport of the GaN solute to the seeds by thermal convection currents, and crystallization of the GaN solute on the seeds. While the total growth rate cannot be theoretically estimated due to the absence of models for dissolution and crystallization, the role of transport can be ascertained. Consequently, in this work we idealize the dissolution and crystallization processes and ascertain the growth rate as determined purely with transport as a determining factor. The growth rate so obtained is termed 'transport determined growth rate'. By comparing the transport determined growth rates with the actual growth rates, we can ascertain whether transport is a limiting factor in the growth. Armed with this tool we further conduct a parametric study to determine the affect of geometric parameters on the transport determined growth rates, and ascertain conditions when transport might be a limiting factor for the growth rate.

2. The ammonothermal process

Fig. 1 shows a schematic of the autoclave for the ammonothermal process. The schematic shows a sealed Rene41 vessel containing supercritical ammonia; a baffle divides the vessel into two chambers. The lower chamber contains a porous bed of GaN powder, and the upper chamber contains seeds of single crystal GaN. The baffle has a central opening and there is a gap between the walls of the autoclave and the baffle. The central opening and the gap serve to enable transport of the solvent (supercritical ammonia) between the two chambers. The autoclave chamber containing ammonia is 9.32 mm in diameter, and 184 mm high. The porous bed at the bottom is 20 mm high, and the baffle another 20 mm above the top of the porous bed. The autoclave is maintained at a temperature between 350 and 600 °C and a pressure of 3–4 Kbar. At these temperatures and pressures the ammonia is in a supercritical state. The supercritical state is characterized by enhanced chemical reactivity and transport properties. More specifically the supercritical state displays the density

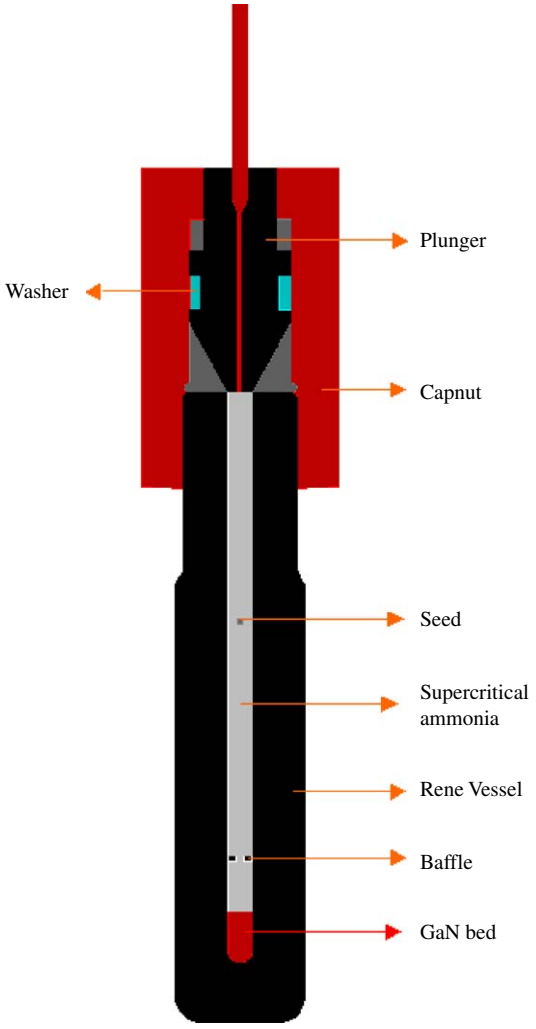

Fig. 1. Schematic of the autoclave assembly. Various parts are indicated in different shades.

associated with a liquid and the viscosity associated with a gas, resulting in enhanced natural convection and solute diffusivities. A mineralizer is added to the supercritical solution to facilitate the dissolution of GaN. A number of different combinations of mineralizers such as KNH_2, KI have been used [5]. Acidic mineralizers like NH_4X; X = Cl, Br, I have also been reported. The lower portion of the autoclave is heated either in a furnace or a band heater arrangement, and buoyancy driven flows are set up. As a result of the action of the supercritical ammonia in conjunction with the mineralizers, the GaN powder in the porous bed dissolves in the form of some intermediates (which are yet to be determined) and is transported by the buoyancy flow to the upper portion of the autoclave. Since the temperature here is lower, and if the solubility decreases with decrease in temperature, the ammonia becomes supersaturated with intermediates, which deposit as GaN on the seeds present in the upper chamber. The role of the baffle separating the upper and lower chamber is to partly obstruct the flow and maintain relative isolation between the two chambers in order to maintain an adequate temperature differential.

3. Model for the ammonothermal process

The main issues in ammonothermal growth may be divided into three broad categories: chemistry, transport and crystallization mechanisms.

3.1. Chemistry and crystallization

The dissolution of the GaN into intermediates by the supercritical ammonia is an open chemical issue. The identity of the intermediates depends on the type and concentration of mineralizers used and the temperature prevailing in and on the top of the GaN porous bed. There is a need for generating equilibrium phase diagrams to identify the intermediates based on the above parameters. Presently, the identity of the intermediates and the kinetics of the dissolution have not been resolved. The crystallization rates again depend on the identity of the intermediates, the structure of the GaN surfaces. A theory of crystallization taking all these factors into account is not yet available. Hence the rate of crystallization and rate of dissolution cannot be modeled in a physically complete sense.

3.2. Transport

Transport can be a determining factor in the growth rate. As already explained transport is driven by the buoyancy convection that is set up due to thermal and density gradients in the supercritical ammonia. The flow and temperature problem is solved by adopting the Boussinesq approximation and solving the Navier–Stokes and energy equation for flow and temperature calculations. The flow was found to be turbulent, and hence a

renormalized group k–ε model was used to model this phenomenon. The equations in the various regions are given below.

Solid region: The autoclave walls, the baffle and the insulation comprise this region. The only equation that needs to be solved is the energy balance or the conduction equation.

$$\text{Energy balance}: \quad \nabla\cdot(\nabla k_s T)=0.$$

Region of supercritical ammonia: The momentum balance, continuity and energy equations have to be solved. The flow in the supercritical region is turbulent, and hence effective viscosities and conductivities have to be used.

Momentum balance:

$$\rho_f \nabla\cdot(\vec{v}\vec{v}) = -\nabla p + \nabla\cdot\left(\bar{\bar{\tau}}\right) - \rho_f\beta_f(T-T_0)\vec{g}$$

Continuity equation:

$$\nabla\cdot(\vec{v})=0$$

Energy equation:

$$(\rho c_p)_f[(\vec{v}\cdot\nabla)T] = \nabla\cdot(k_{eff}\nabla T).$$

Nutrient zone: The nutrient zone is the porous bed of ammonia. The Darcy–Brinkman–Forschheimer model is used to estimate the additional forces on the fluid due to a porous medium, and the effective thermal conductivity.

Momentum balance:

$$\rho_f \nabla\cdot(\vec{v}\vec{v}) = -\nabla p + \nabla\cdot\left(\bar{\bar{\tau}}\right) - \rho_f\beta_f(T-T_0)\vec{g} - \frac{\mu_f}{K}\vec{v} - \frac{1}{2}C_2\rho_f|\vec{v}|\vec{v}$$

Continuity equation:

$$\nabla\cdot\vec{v}=0$$

Energy equation:

$$(\rho c_p)_f[(\vec{v}\cdot\nabla)T] = \nabla\cdot(k_{por}\nabla T)$$

$$k_{por}=\varepsilon_{bed}k_{eff}+(1-\varepsilon_{bed})k_s; \quad K=\frac{d_p^2\varepsilon_{bed}^3}{150(1-\varepsilon_{bed})^2};$$

$$C_2=\frac{3.5(1-\varepsilon_{bed})}{d_p\varepsilon_{bed}^3}.$$

Renormalized group k–ε model: This model introduces the turbulent fluctuations kinetic energy k, and the turbulent dissipation rate ε, and calculates the turbulent viscosity, conductivity and other transport quantities in terms of these quantities.

k-equation:

$$\frac{\partial}{\partial t}(\rho_f k)+\nabla\cdot(\rho_f k\vec{v}) = \nabla\cdot(\alpha_k\mu_{eff}\nabla k) + G_k + G_b - \rho\varepsilon$$

ε-equation:

$$\frac{\partial}{\partial t}(\rho_f\varepsilon)+\nabla\cdot(\rho_f\varepsilon\vec{v}) = \nabla\cdot(\alpha_\varepsilon\mu_{eff}\nabla\varepsilon) + C_{1\varepsilon}\frac{\varepsilon}{k}(G_k+C_{3\varepsilon}G_b) - C_{2\varepsilon}\rho\frac{\varepsilon^2}{k} - R_\varepsilon$$

Effective viscosity equation:

$$\mu_{eff}=\mu_f+\frac{\rho_f C_\mu k^2}{\varepsilon};$$

$$C_\mu = 0.0845$$

Source terms in the k- and ε-equations:

$$G_k = \tfrac{1}{2}(\mu_{eff}-\mu_f) \times[(\vec{\nabla}\vec{v}+\vec{v}\overleftarrow{\nabla}):(\vec{\nabla}\vec{v}+\vec{v}\overleftarrow{\nabla})]$$

$$G_b=\beta_f\frac{\mu_{eff}-\mu_f}{Pr_t}\nabla T\cdot\vec{g}$$

$$R_\varepsilon=\frac{C_\mu\rho_f\eta^3(1-\eta/\eta_0)}{1+\beta\eta^3}\frac{\varepsilon^2}{k};$$

$$\eta=0.5[(\vec{\nabla}\vec{v}+\vec{v}\overleftarrow{\nabla}):(\vec{\nabla}\vec{v}+\vec{v}\overleftarrow{\nabla})]\frac{k}{\varepsilon}; \quad \eta_0=4.38;$$

$$\beta=0.012 \quad \alpha_k=\alpha_\varepsilon$$

and are calculated from

$$\left|\frac{\alpha_k-1.3929}{1-1.3929}\right|^{0.6321}\left|\frac{\alpha_k+2.3929}{1+2.3929}\right|^{0.3679}=\frac{\mu_f}{\mu_{eff}}$$

Pr_t is calculated from

$$\left|\frac{1/Pr_t-\mu_f(c_p)_f/k_f}{1-1.3929}\right|^{0.6321}\left|\frac{1/Pr_t+\mu_f(c_p)_f/k_f}{1+2.3929}\right|^{0.3679}=\frac{\mu_f}{\mu_{eff}}$$

$$k_{eff}=k_f+(c_p)_f(\mu_{eff}-\mu_f)/Pr_t$$

$$C_{1\varepsilon}=1.42 \text{ and } C_{2\varepsilon}=1.68$$

Boundary conditions, technique and properties: Since, the mesh near the boundaries is not fine enough, wall functions are used to estimate shear stress parallel to the wall, τ_w, and use it in the momentum equation near the walls to obtain a boundary condition. The wall conditions for the momentum equation are:

$$U^*=(U_P C_\mu^{1/4}k_P^{1/2})/(\tau_w/\rho); \quad y^*=(\rho C_\mu^{1/4}k_P^{1/2}y_P)/\mu_f;$$

$$U^*=y^*; \quad \text{if } y^*\leqslant 12$$

$$U^*=2.38\ln(9.81y^*); \quad \text{if } y^*>12$$

U_P is the velocity parallel to the wall at point 'P'; y_P is normal distance from wall.

Similarly, wall functions to estimate the heat flux normal to a wall, and use it in the energy balance equation: $T^*=((T_w-T_P)\rho_f(c_p)_f C_\mu^{1/4}k_P^{1/2})/q_w$

$$T^*=Pr\,y^*; \quad \text{if} \quad y^*\leqslant y_T^* \tag{i}$$

$$T^*=Pr_t[2.38\ln(9.81y^*)+P]; \quad \text{if } y^*>y_T^* \tag{ii}$$

Table 1
Properties of supercritical ammonia used in the simulations

Density	Specific heat capacity	Thermal conductivity	Viscosity	Thermal expansion coefficient
447 kg/m^3	2519 J/kg K	0.33 W/m K	5.7e–05 m^2/s	0.00135 /K

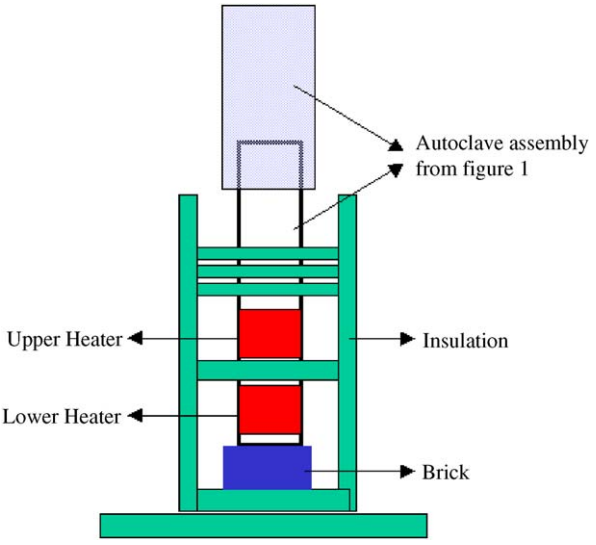

Fig. 2. Complete heating arrangement of the autoclave. The temperature of the upper and lower heater is controlled.

$$\mathrm{Pr} = (\mu c_p)_f / k_f$$

$$P = 9.24\left[\left(\frac{\mathrm{Pr_t}}{\mathrm{Pr}}\right)^{3/4} - 1\right]\left[1 + 0.28\mathrm{e}^{-0.007\mathrm{Pr_t}/\mathrm{Pr}}\right],$$

y_T^* is determined by plotting (i) and (ii); the intersection of these two curves is at y_T^*.

Boundary conditions are required for k and ε at the walls. The formula for turbulence dissipation at cell centers 'P' adjacent to boundary nodes—$\varepsilon_P = C_\mu^{3/4} k_P^{3/2}/(0.4128 * y_P)$ provides the boundary condition for turbulent dissipation, while the turbulent kinetic energy follows the Neumann condition $\nabla k \cdot \vec{n} = 0$. The technique adopted to solve flow temperature and other fields is the finite volume method along with an unstructured discretization and the SIMPLE algorithm due to Patankar [9]. The flow, temperature and other fields are assumed to be axisymmetric. Before calculations are set up, major issues are the thermal boundary conditions that are to be set up for the calculations and the transport properties of the supercritical ammonia. Transport properties were obtained from the NIST database—at average pressure and temperature estimated in the autoclave—and are summarized as shown in Table 1. To specify the proper thermal boundary conditions the full heating arrangement needs to be known. This is shown in Fig. 2, and apart from the insulation and other artifices, basically consists of two strip heaters all configured around the autoclave. The boundary conditions to be determined are the convective coefficients on all the surfaces exposed to the ambient assumed to be at room temperature—25 °C. The temperatures on both the strip heater surfaces are also specified. The thermal conductivities of all the materials used in the configuration of Fig. 2 were obtained from the manufacturers tables. To gauge the convective coefficients on the surfaces exposed to the ambient, the following procedure was used. In experiments conducted by our collaborators, the autoclave was filled with air instead of supercritical ammonia. The power in the heaters was so adjusted as to fix the temperature of both the heaters at predetermined values and the profile along the centerline of the autoclave measured. This arrangement was then simulated with the temperature of the heaters fixed at set values and the convective coefficients at the boundaries adjusted so that the simulated profile along the centerline is close to the experimental one. The thermal response of the system is thus calibrated and the boundary conditions determined.

3.3. Transport determined growth rate

As mentioned before, the growth rate is controlled by the sequence of (1) dissolution of GaN, (2) transport of the dissolved species from the nutrient zone to growth zone, and (3) crystallization of the dissolved species on the growing crystal. Since theories for the rates of dissolution and crystallization are not available yet, we propose an idealization of these phenomena, and consider only the role of transport in the growth. This is facilitated by the availability of equilibrium solubility curves for GaN in supercritical ammonia. These curves are again influenced by the nature and concentration of the mineralizer. A series of three such curves are shown in Fig. 3. Curve 2 shows some interesting features even demonstrating retrograde solubility of GaN with temperature in certain ranges. A boundary value problem (BVP) can now be set up, by solving the diffusive-convective equation for the transport of GaN (actually intermediate). In the porous bed and on the surface of the seed the concentration of the GaN can be set as a boundary condition, by prescribing it as a function of the temperature as given by the equilibrium solubility curve. The required equation is

$$\frac{\partial}{\partial t}(\rho_f C) + \nabla \cdot (\rho_f \vec{v} C) = D_{\mathrm{eff}} \nabla^2 C, \tag{1}$$

where C is the GaN (intermediate) concentration expressed as mass of intermediate/mass of ammonia solvent, ρ_f the density of supercritical ammonia. The boundary conditions are indicated in Fig. 4, where $f(T)$ refers to concentration at

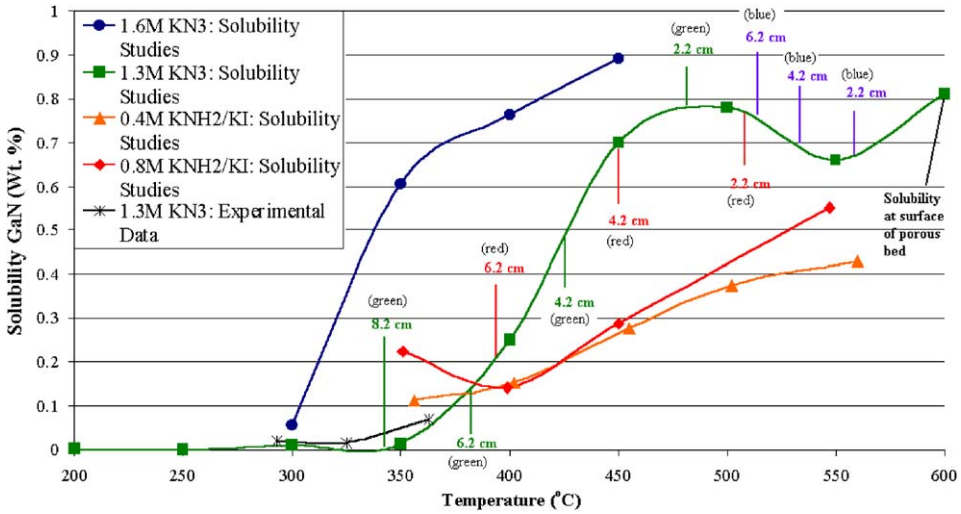

Fig. 3. Solubility of GaN in supercritical ammonia as a function of temperature for different mineralizers. (Figure obtained courtesy of Prof. Joseph Kolis, Department of Chemistry, Clemson University).

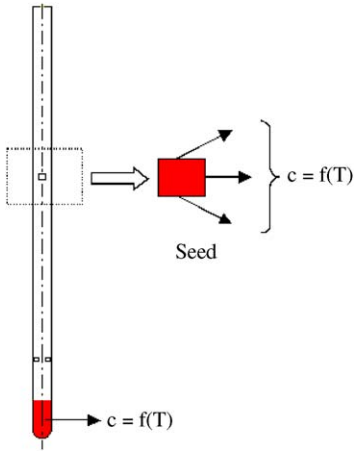

Fig. 4. A depiction of the concentration boundary conditions inside the porous bed (colored in red) and on the surface of the seed (zoomed view colored in red). $f(T)$ is the variation of equilibrium solubility with temperature as can be read from the plots of Fig. 3.

the boundaries as a function of temperature as given by the solubility curve.

The effective diffusion coefficient of the solute D_{eff} is a sum of the laminar diffusion coefficient D_{lam} and the considerable enhancement due to turbulence D_{turb}. The correlation of He–Yu [10] was used to estimate the laminar contribution:

$$\frac{D_{\text{lam}}}{\rho_{\text{f}}} = A \times 10^{-9}\sqrt{\frac{T}{M}}\exp\left\{\frac{-0.3887V_{\text{c}}}{V-0.23V_{\text{c}}}\right\};$$
$$A = 14.882 + 5.9081k + 2.0821k^2; k = T_{\text{c}}V_{\text{c}}.$$

The relevant quantities required for use in the correlation are: $V_{\text{c}} = 4.444 \times 10^{-3}\,\text{m}^3/\text{kg}$, $T_{\text{c}} = 405.40\,\text{K}$, $V = 1/\rho_{\text{f}} = 2.237 \times 10^{-3}\,\text{m}^3/\text{kg}$. The molecular weight of the intermediate species in solution M was assumed to be 150 gm/mole. This correlation gives an estimate of the laminar diffusion coefficient. In reality, the flow inside the autoclave cavity might be turbulent and the contribution to D_{turb} might swamp the laminar contribution. D_{turb} is estimated by means of a turbulent Schmidt number assumed to have a value of 0.7. Hence $D_{\text{turb}} = (\mu_{\text{eff}} - \mu_{\text{f}})/0.7$. The 0.7 value for the turbulent Schmidt number is an estimate and is close to the value prevalent for a number of solutes in turbulent flows. We find in our simulations that D_{turb} swamps D_{lam}, and hence D_{eff} is almost equal to D_{turb}. However, near the seed boundary, the fine mesh in the ammonia (0.4 mm) resolves the laminar sublayer within the turbulent boundary layer, and hence D_{eff} is almost equal to D_{lam} in the finite volume elements within the boundary layer near the seed.

The BVP for the solute concentration is well posed. The strategy adopted is to solve the steady state Navier–Stokes and energy equations to obtain the steady state temperature and velocity fields. Once this is accomplished the unsteady Eq. (1) can be integrated in time along with the boundary conditions till the steady state concentration field is obtained; calculation of the flux at the seed surface at any instant of time leads to an estimate of the transport determined growth rate as a function of time. The above analysis implicitly assumes that the thermal and flow fields develop faster than the concentration field, but the assumption does not have any effect on the result for the final steady-state growth rates.

The growth rate histories have been evaluated for different conditions by varying (1) the temperature of the upper strap heater (2) the location of the seed in the autoclave (3) and the baffle design. These affect the transport and the temperature at the seed location and directly affect the growth rate.

4. Results and discussion

The properties of other materials involved in the calculations like Rene 44, solid GaN, etc., were obtained

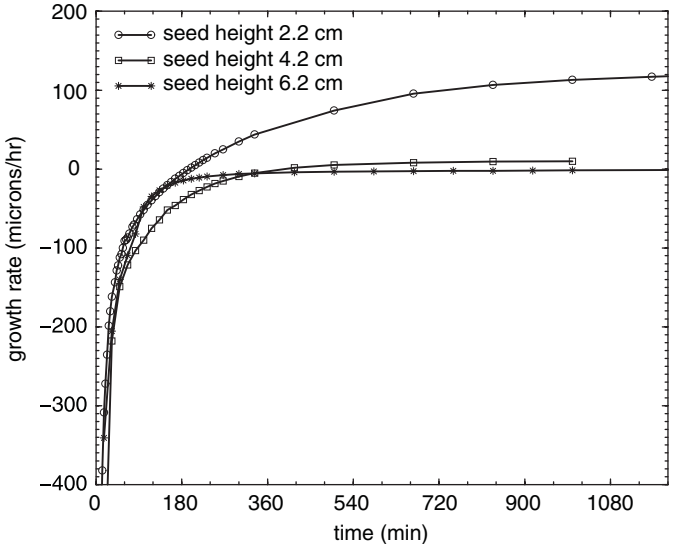

Fig. 5. Transport determined growth rate evolution for the seed at different heights above the baffle. Temperature of upper heater: 550 °C, lower heater: 600 °C.

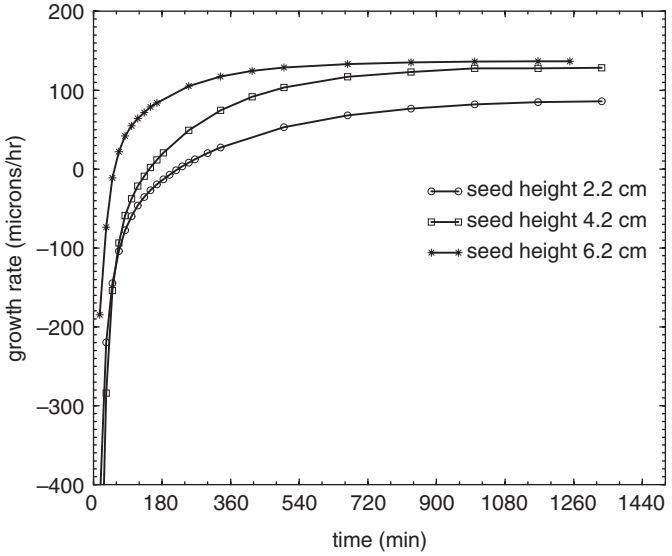

Fig. 6. Transport determined growth rate evolution for the seed at different heights above the baffle. Temperature of upper heater: 450 °C, lower heater: 600 °C.

from standard literature. The porous properties of the nutrient layer were calculated by assuming a particle diameter of 0.8 mm, and a porosity of 0.4. The autoclave chamber containing ammonia is 9.32 mm in diameter, and 184 mm high. The porous bed at the bottom is 20 mm high, and the baffle another 20 mm above the top of the porous bed. The temperature of the upper heater and the seed location are varied first. Fig. 5 shows the growth history with the lower heater at 600 °C and the upper heater at 550 °C. The height of the seed above the baffle was varied to 2.2, 4.2 and 6.2 cm. In all three cases the steady state growth rates are obtained between 5 and 15 h. The growth rates are negative for the first few hours. This is because in this interval, the GaN transport from the bed to the seed is still developing and hence the seed experiences dissolution. The final steady-state growth rates are partly driven by the difference in the solubility corresponding to the temperatures at the top of bed and the surface of the seed. The solubility at the seed surface for the three cases is indicated in blue color on the solubility versus temperature curve in Fig. 3. The solubility on top of the porous bed is also indicated. Due to the retrograde solubility in this region, the solubility difference driving the growth rate is highest for seed height of 2.2 cm, even though the seed surface is at the highest temperature in this case. The solubility difference was lower for the 4.2 cm and lowest for 6.2 cm seed heights. The steady-state growth rates follow the same order.

The temperature of the lower heater is then lowered to 450 °C. Fig. 6 shows the results in this case. The final growth rates for seed heights of 6.2 and 4.2 mm are close together while the growth rate in the 2.2 mm case is lower. Fig. 3 shows the solubility at temperatures corresponding to the top of the GaN bed and the seed surface for the three different cases in letters of red color. Though the solubility

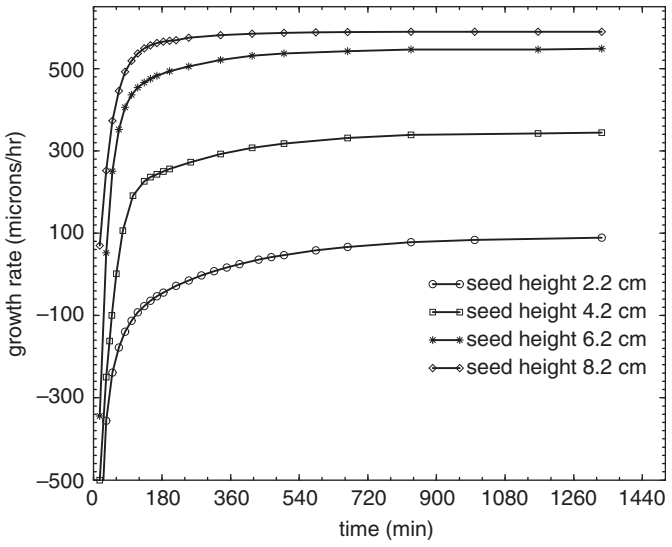

Fig. 7. Transport determined growth rate evolution for the seed at different heights above the baffle. The temperature of the upper heater is not fixed and the lower heater is at 600 °C.

difference in the 6.2 mm case is much higher than that in the 4.2 mm case, the final steady-state growth rates are nearly similar. This suggests that in these two cases transport is a limiting factor. The final growth rate is constrained by the amount of solute the solvent can transport from the bed to the seed surface.

The temperature of the upper heater is then set free to stabilize (physically this corresponds to no heating in the upper heater), and the lower heater maintained at 600 °C as before. The results are shown in Fig. 7. The final growth rates again follow the solubility difference as dictated by the solubility at the surface of the seed. These are presented

in Fig. 3 in letters of green color. Following the trend in the solubility difference, the final steady-state growth rates show a steady increase from 2.2 to 4.2 to 6.2 cases, but the growth rates in 6.2 and 8.2 cases are nearly identical. This is similar to the trend when the temperature in the lower heater was 450 °C and suggests again that transport is a limiting factor. The final growth rates are determined by two factors: the concentration boundary conditions on the surface of the seed, and the transport. The concentration boundary conditions are determined by the temperature field, and are expressed through the solubility difference. Changing the position of the seed affects the temperature at the seed surface, and consequently the concentration boundary condition. In general, higher the seed, lower its temperature and the equilibrium concentration at that temperature (except in special cases of retrograde solubility between temperatures 500 and 550 °C in Fig. 3). Consequently, a greater solubility difference drives the growth when the seed is higher. This is reflected in higher growth rates in Figs. 6 and 7 when the seed is higher. However, once the seed height exceeds a certain value the growth is saturated; solubility difference no longer determines the growth. Transport is then the limiting factor. Transport is determined by the flow field, which is in turn driven by the temperature difference between the upper and the lower heaters. The lower the temperature of the upper heater, the greater the temperature difference driving the flow and higher the transport. This is also reflected in the growth rates by a comparison growth rates in Figs. 5–7 for the same seed heights.

The next design consideration is the baffle. The primary purpose of the baffle is to maintain an adequate temperature differential between the GaN nutrient bed and the seed. At the same time, the baffle obstructs transport; its role is thus unclear. Simulations were carried out with no baffle and three different baffle dimensions. A view of the inner cavity of the autoclaves with different baffle designs is shown in Fig. 8. Fig. 8(b) shows an autoclave without a baffle, Fig. 8 (a), (c) and (d) show autoclaves with increasingly bigger baffles. Fig. 9 shows the growth rate histories for these configurations. In this simulation, the seed height is 2.5 cm, the lower heater temperature is set at 600 °C, and the upper heater temperature is set at 550 °C. The difference in steady-state growth rate for all four cases is marginal. It is highest for baffle '*a*', and decreases very marginally when the size of the baffle is increased to '*c*', and further decreases when the size of the baffle is increased to '*d*'. A bigger baffle suppresses flow and hence transport. In case '*b*' with no baffle, the growth rate is lower than the growth rate with baffle '*a*', but higher than the growth rate for the larger two baffles.

The above analysis was repeated with a new seed height of 6.5 cm and without fixing the temperature of the upper heater. Fig. 10 shows the growth rate histories for three baffles. The trends are similar to Fig. 9, but more pronounced due to more transport. The highest growth

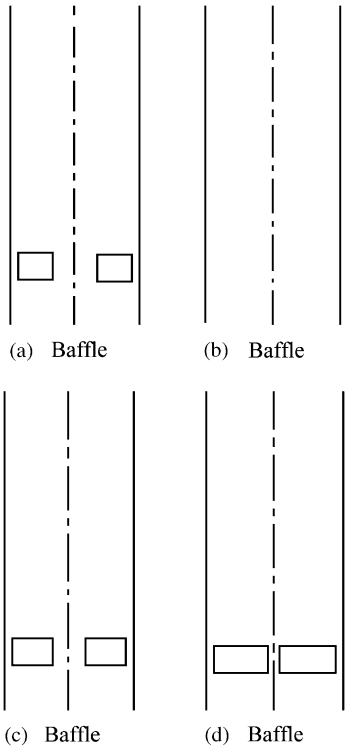

Fig. 8. Different baffle dimensions: (a) diameter of central opening is 3.10 mm, (b) no baffle, (c) diameter of central opening is 2.32 mm, (d) diameter central opening is 1.2 mm. The gap between autoclave wall and baffle is 0.7 mm. The line in the center of each figure is the 'centerline' and is not a physical object.

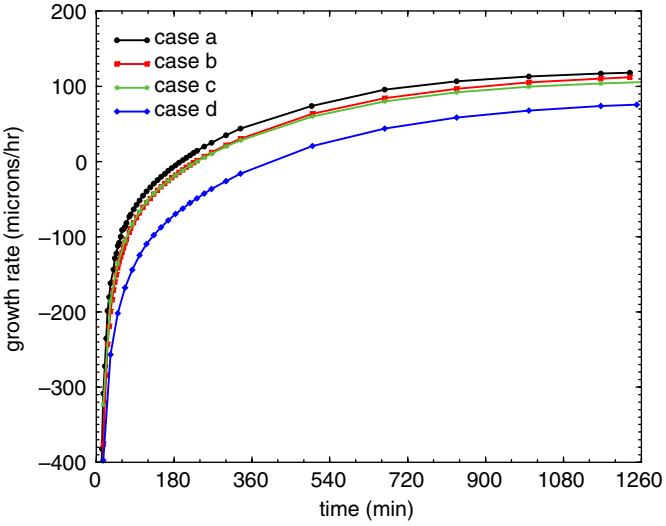

Fig. 9. Transport determined growth rates for the four different baffle configurations of Fig. 8. The lower heater is at 600 °C, upper heater at 550 °C, and the seed height above baffle is 2.5 cm.

occurs for baffle '*a*' and decreases in '*d*' due to choking of fluid flow by larger baffle. The case '*b*' without a baffle also produces less growth than baffle '*a*'. This confirms the original intent of a baffle. The absence of a baffle increases the temperature of the surface of the seed and decreases the solubility difference driving the growth. Hence the growth

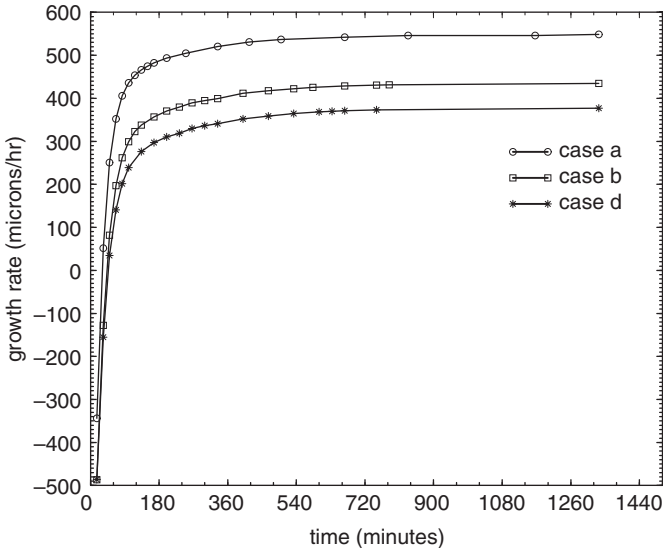

Fig. 10. Transport determined growth rates for the four different baffle configurations of Fig. 8. The lower heater is at 600 °C, upper heater temperature free, and the seed height above baffle is 6.5 cm.

rate decreases when there is no baffle. The analysis confirms that the presence of a baffle is beneficial, but the dimensions of the baffle have to be carefully adjusted to produce the right balance of transport and super-saturation at the surface of the seed.

It is important to focus on the numbers for the growth rates. These are of the order of tens to hundred of microns an hour, while in real experiments the growth rates are of the order of hundreds of microns a day. This discrepancy can be explained by pointing out that the growth rates above are transport determined growth rates, and have been obtained after idealizing dissolution and crystallization kinetics. It suggests that crystallization and dissolution kinetics are the bottlenecks for growth at the present stage. These are chemistry issues and have to be tackled first to get a decent growth rate. Once these are resolved, more analysis such as above can be used to fine-tune the process.

5. Conclusion

A computational model for the ammonothermal growth of bulk single crystal GaN has been constructed. Apart from solving for flows and temperature, a transport determined growth model and 'transport determined growth rate' are proposed by idealizing the process of dissolution and crystallization. The transport determined growth rates thus obtained were an order of magnitude higher than the actual ones, suggesting that dissolution and crystallization kinetics and not transport are the growth limiting factors. However, circumstances have been identified when transport can be a limiting factor. The role of the baffle has also been clarified.

The transport limited growth rate is primarily driven by (1) the solubility difference between the top of the bed and the surface of the seed (2) the transport. The solubility difference primarily depends on the temperature field and the placement of the seed. For a given flow field, the maximum growth rate is restricted by the amount of solute that the flow field is intrinsically capable of transporting. For low solubility differences, transport is not a factor, but once the solubility difference driving the growth increases, transport increasingly presents a bottleneck and ultimately saturates the growth rate. The design of the baffle is again an outcome of the competing influences of solubility difference and transport. Too large a baffle opening, or the absence of a baffle decreases the temperature difference between the nutrient and the seed, while too small a baffle opening chokes the flow and the transport. Either extreme is bad for the growth rate. Thus an optimum baffle configuration exists and has been tentatively determined.

The above methodology provides a clear-cut procedure to optimize the evolving ammonothermal growth equipment in terms of maximizing transport and tailoring the flow and temperature fields in accordance with solubility curves. As the solubility data improves and matures, this methodology will become more effective and reliable.

Acknowledgments

We wish to thank Michael Callahan of AFRL Laboratories, Hanscom, USA, and Prof. Joseph Kolis, Department of Chemistry, Clemson University, USA for some of the material. This work was supported by ONR via North Carolina State University as part of the MURI on "Growth and Wafering of Bulk III-Nitrides" (Contract Grant Moniter Dr. Colin Wood).

References

[1] S. Porowski, I. Gregory, J. Crystal Growth 178 (1–2) (1997) 174.
[2] H. Yamane, M. Shimada, S.J. Clarke, F.J. DiSalvo, Chem. Mater. 9 (2) (1998) 413.
[3] R. Dwilinski, J.M. Baranowski, M. Kaminska, R. Doradzinski, J. Garczynski, L. Sierzputowski, Acta Phys. Pol. A 90 (4) (1996) 763.
[4] R. Dwilinski, R. Doradzinski, J. Garczynski, L. Sierzputowski, M. Palczewska, A. Wysmolek, M. Kaminska, MRS Internet J. Nitride Semicond. Res. 3 (1998) article 25.
[5] D.R. Ketchum, J.W. Kolis, J. Crystal Growth 222 (3) (2001) 431.
[6] A.P. Purdy, Chem. Mater. 11 (7) (1999) 1648.
[7] A. Yoshikawa, E. Ohshima, T. Fukuda, H. Tsuji, K. Oshima, J. Crystal Growth 260 (1–2) (2004) 67.
[8] B. Raghothamchar, W.M. Vetter, M. Dudley, R. Dalmau, R. Schlesser, Z. Sitar, E. Michaels, J.W. Kolis, J. Crystal Growth 246 (3–4) (2002) 271.
[9] S.V. Patankar, Numerical Heat Transfer and Fluid Flow, Hemisphere Publishing Corporation, Washington, McGraw-Hill, New York, 1980.
[10] C.H. He, Y.S. Yu, Ind. Eng. Chem. Res. 37 (1998) 3793.